Novel regulators of endosome dynamics, MHCII antigen presentation and chemosensitivity

Wijdeven, R.H.M.

Chapter 4:
Identification of DUBs controlling MHCII biology and endosome dynamics.

Ruud H. Wijdeven[1,2], Ilana Berlin[1,2], George Jansen[3], Hans Janssen[2], Peter van Veelen[3], Jacques Neefjes[1,2]

[1] Department of Chemical Immunology, LUMC, Leiden, the Netherlands
[2] Department of Cell Biology, Netherlands Cancer Institute, Amsterdam, the Netherlands
[3] Department of Immunohematology and Blood Transfusion, LUMC, Leiden, the Netherlands.

Abstract

For efficient antigen loading and presentation at the cell surface, MHC class II molecules (MHCII) traverse an extensive part of the endocytic pathway. Interference with the latter could be used as means to manipulate MHCII antigen presentation, and hereby the activation of CD4+ T-cells. Here, by performing an RNAi screen for de-ubiquitinating enzymes (DUBs), we identified novel functions in the MHCII pathway for several of these enzymes. One of these, OTUD1, regulates transcription of MHCII and is required for proper perinuclear localization of the early and late endosomal compartment. Furthermore, loss of OTUD1 impairs the processing of endocytic cargo, as measured by decreased degradation of endocytosed EGFR. Together, our work provides a framework for future studies on the role of several DUBs in the endocytic pathway and describes a function for OTUD1 in the regulation of the early and late endosomal compartment.

Introduction

Antigen presenting cells (APCs) activate CD4+ helper T-cells to initiate an adaptive immune response by presenting antigens on their Major Histocompatibility Complex class II molecules (MHCII) (1, 2). Improper antigen presentation or undesired stimulation of autoreactive CD4+ T-cells underlies many autoimmune diseases, and multiple MHCII alleles associate to specific autoimmune disorders, for example HLA-DRB1 and rheumatoid arthritis and HLA-DR4 to Type I Diabetes (3, 4). Expression of MHCII is limited to professional APCs like dendritic cells and B-cells, but other cell types can also express MHCII upon cytokine stimulation or oncogenic transformation. Transcription of the MHCII complex (consisting of an alpha and beta chain, as well as the invariant chain (Ii) that is required for peptide loading and endosomal trafficking) is controlled by transcriptional activator CIITA, which recruits the necessary transcription factors to initiate transcription (5). After synthesis in the ER, MHCII associates with Ii, followed by transport via the trans-Golgi network (TGN) to multi-vesicular late endosomes, also called MHCII compartments (MIIC). Alternatively, MHCII is first transported towards the plasma membrane and subsequently endocytosed to reach the MIIC. Here, the invariant chain is cleaved by various proteases including cathepsin S and SPPL2a (6, 7), leaving only a small fragment termed CLIP in the MHCII peptide-binding groove. Subsequent association of CLIP-bound MHCII with chaperone HLA-DM facilitates exchange of CLIP for an external peptide (8). Most peptides are generated in endosomes, but cytosolic and even nuclear peptides are presented by MHCII, usually after they entered the MIIC by autophagy (9, 10). After loading, MHCII is transported to the cell surface, where the peptide is presented.

While the basic principles of antigen presentation are set, the underlying processes ensuring proper expression and transport of MHCII are understood less well. Furthermore, as it utilizes major parts of the endocytic pathway, MHCII is an excellent marker for the identification of novel members of this cellular trafficking system. A group of enzymes that could control these processes are de-ubiquitinating enzymes (DUBs), which counteract post-translational modification (PTM) of proteins by ubiquitin (11). Ubiquitination is one of the most prevalent PTMs and is involved in almost every cellular process, ranging from targeting proteins for proteasomal

degradation to signal transduction (12). Proteins can be modified on a lysine with a single ubiquitin (mono-ubiquitination), which can further be ubiquitinated, leading to the formation of ubiquitin chains (poly-ubiquitination). Depending on the lysine on ubiquitin that is modified, this yields chains with different structures and functions. DUBs cleave off the ubiquitin (chain), thereby preventing protein degradation or terminating the ubiquitin-based signal. Given the reversible and flexible nature of PTMs in the endocytic pathway, DUBs perform essential functions in trafficking, reaching beyond modulation of protein abundance (13, 14). As MHCII molecules traverse nearly the entire endocytic network, DUBs implicated in endocytic trafficking, including USP8 and AMSH (15), could influence MHCII expression. Also, many DUBs are poorly studied and some may be involved in endocytic trafficking or transcription of MHC-related genes. Their enzymatic nature makes them attractive drug targets to modulate the magnitude of antigen presentation.
To identify novel regulators of MHCII expression and endocytic transport in general, we performed an RNAi screen for the different de-ubiquitinating enzymes. Using this screen, we identified several DUBs that control MHCII surface expression, either by regulating transcription or endocytic trafficking. One of these DUBs, OTUD1, was studied in more detail. OTUD1 is required for transcription of MHCII, as well as for proper localization of the late endosomal/lysosomal (LE/Ly) compartment, suggesting a pleiotropic function for this lysine-63 specific DUB.

Results

RNAi screen for DUBs in control of MHCII expression

Cell surface levels of MHCII are regulated by a plethora of factors, with many of them uncovered by a genome-wide RNAi screen performed in our lab (16). However, only few DUBs were identified in this screen, likely due to its stringent selection criteria and large scale. As some DUBs implicated in endocytic trafficking were not identified, we performed a more targeted screen using a library of siRNAs targeting all known DUBs. As a model for MHCII expression the MelJuSo melanoma cell line was used, which constitutively expresses the MHCII transcriptional regulator CIITA at high levels and is transfectable. DUBs were silenced for three days to allow sufficient knockdown, after which cell surface levels of peptide loaded MHCII were measured using flow cytometry (Fig. 1a).
Silencing of 9 DUBs increased MHCII expression (z-score >2.5), whereas depletion of 11 DUBs yielded a decrease in MHCII cell surface levels (Fig. 1b). To assess whether any of these DUBs are in control of MHCII transcription, the DUBs were silenced and cells were subjected to qRT-PCR analysis for MHCII subunit HLA-DRα. Depletion of USP9x, USP42, as well as the OTU-domain DUBs OTUD1 and OTUD4 decreased HLA-DRα transcription (Fig. 1c). Of these four DUBs, only depletion of OTUD1 quenched HLA-DRα expression induced by the cytokine IFNγ (Fig. 1d). Transcription of Ii, which is co-regulated with OTUD1, or CIITA and IRF1, were not affected by OTUD1 knockdown, suggesting that OTUD1 is specifically involved in transcription of HLA-DRα.
MHCII extensively traverses the endocytic network and some DUBs may affect its surface levels by altering transport. Confocal microscopy for MHCII, as well as GFP-tagged ubiquitin to investigate ubiquitin dynamics, revealed that whereas the

perinuclear accumulation of MHCII remained intact after silencing of most DUBs, silencing of some DUBs severely affected the localization or size of the MIIC compartment (Fig. 1e). Depletion of USP8 induced swelling of the MIIC, which was heavily labeled with ubiquitin, consistent with the known role for USP8 in trafficking of receptors through the endocytic compartment (17, 18). Loss of USP34 yielded hyperclustering of the MIICs, while USP54 silenced cells had hyperclustered MIICs in combination with increased plasma membrane staining, which agrees with the Flow Cytometry data. Increased plasma membrane staining was also observed for depletion of VCPIP. Finally, loss of USP9x and OTUD1 resulted in scattering of MHCII throughout the cell, as well as the appearance of ubiquitin aggregates in the cytosol, which were also visible when USP54 was silenced. The decreased MHCII surface levels as a result of OTUD1 knockdown were a result of impaired MHCII transcription and not trafficking, as total MHCII levels were also altered, overexpression of GFP-tagged HLA-DRα driven by a CMV promotor rescued MHCII surface levels, and cell surface expression of CD63, which also localizes to LE/Lys, was not affected by OTUD1 silencing (Fig. 1f). Thus, we identified several novel DUBs that control transcription and/or transport of MHCII.

OTUD1 is required for late endosome positioning

One of the interesting hits was OTUD1, a DUB specifically cleaving lysine-63 poly-ubiquitin linkages (19) and overexpressed in early stages of thyroid cancer (20). However, its cellular function is unknown. The re-localization of MHCII upon silencing of OTUD1 suggests that this DUB might be involved in trafficking of LE/Lys. Indeed, silencing of OTUD1 using two different siRNAs resulted in a profound scattering of CD63-positive compartments in both HeLa and MelJuSo cells (Fig. 2a). Overexpression of Rab7-effector RILP re-established the perinuclear localization of CD63 (Fig. 2b), suggesting that the peripheral re-localization is not the result of defective minus-end transport towards the perinuclear region. Increased scattering was accompanied by an increase in the number of LE/Lys as stained by CD63 and Lysotracker (Fig. 2c), instilling the idea that OTUD1 is required for proper organization of the endosomal compartment. To address whether these scattered endosomes are a consequence of increased plus-end transport or peripheral stabilization, we labeled these endosomes with lysotracker and followed them by time lapse imaging. Vesicles in the peripheral region did not undergo increased fast microtubule-based transport, indicating that the peripheral re-localization is not a result of increased plus-end transport. Rather, they appeared static and mostly immobile, as if docked to a cellular structure (Fig. 2d and 2e). Thus, OTUD1 affects the organization of the LE/Ly compartment and its loss results in a collapse of the perinuclear region, without increasing actual endosome transport.

Proper endocytic functioning requires OTUD1

To address the effect of OTUD1 on the endosomal pathway as a whole, we stained cells either or not silenced for OTUD1 with markers for different endosomal compartments. Excessive scattering was also observed for early endosomes (detected by EEA1) but not the trans-Golgi network (Mannose-6-phosphate receptor) (Fig. 3a), indicating that OTUD1 acts as a regulator of the early and late endocytic network, but not the entire endocytic pathway that includes TGN.

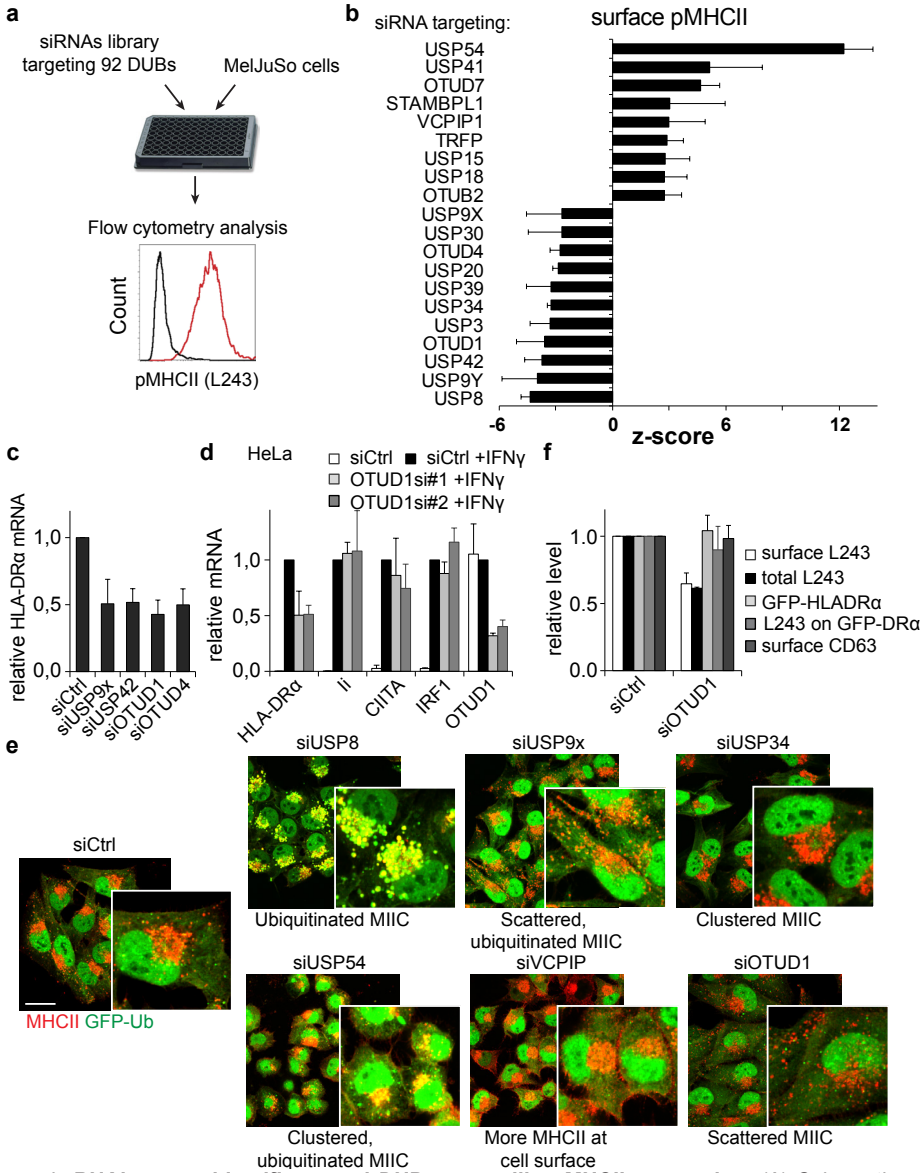

Figure 1: RNAi screen identifies novel DUBs controlling MHCII expression. *(A) Schematic overview of the screen (B) Hits from the screen with a Z-score > 2.5 or < -2.5. Z-scores represent amount of standard deviations away from the control. (C) MelJuSo silenced for hits from the screen were analysed for mRNA expression of HLA-DRα using qRT-PCR. Silencing of four DUBs had a significant effect and are shown. (D) HeLa cells transfected with the indicated siRNAs were stimulated with 100ng/mL IFNγ for 24h and expression of the indicated mRNAs was analyzed using qRT-PCR. (E) MelJuSo cells expressing GFP-Ubiquitin were transfected with the indicated siRNAs and fixed and stained three days later for MHCII. Representative images are shown. Scale bar, 10µm. (F) MelJuSo cells transfected with siCtrl or siOTUD1 were stained for surface pMHCII, CD63 or first fixed and permeabilized to stain for total pMHCII levels. Alternatively, MelJuSo cells expressing GFP-tagged HLA-DRα were stained with L243 and analyzed by flow cytometry for GFP and surface pMHCII levels. All graphs represent mean + SD of three independent experiments.*

Perinuclear localization of endosomes aides the efficient encounter of early endosomes and LE/Lys and hereby times the degradation of cargo, for example activated growth receptors (21). Therefore, we tested the participation of OTUD1 in the timely degradation of the Epidermal Growth Factor Receptor (EGFR). In line with the disorganized endosome localization, ligand-induced degradation of EGFR was delayed upon depletion of OTUD1, which was accompanied by prolonged presence of phosphorylated EGFR (Fig. 3b). The setback in degradation was a result of impaired access of EGFR to the degradatory LE/Ly compartment, since co-localization between fluorescent EGF and CD63 was lower in cells lacking sufficient OTUD1 (Fig. 3c). Whereas in control cells EGF containing endosomes moved towards the perinuclear region, EGF containing endosomes remained dispersed over the cell following OTUD1 silencing, further supporting the notion that OTUD1 is involved in the positioning of endosomes.

OTUD1 is functionally linked to the actin cytoskeleton

Whereas the phenotype suggests an important function for OTUD1 in endosome biology, OTUD1 localized predominantly to the cytosol (Fig. 4c), suggesting an indirect effect on endosomes, possibly via adaptor proteins. An earlier study did not show any endosome associated target (22), therefore we performed mass spectrometry analyses of OTUD1 associated proteins. We isolated GFP-tagged OTUD1 from Hek 293T cells and analyzed interacting proteins by MS/MS. Besides all six reported proteins, peptides were identified corresponding to several novel interactors (Fig. 4a). However, none of these proteins were known to localize to endosomes. Therefore we focused on Filamin A (FLNA), an actin cross-linking protein, as it is described to be required for proper localization of the LE/Ly compartment (23). OTUD1 indeed interacted with Filamin A, via its alanine-rich N-terminal domain (Fig. 4b). Given the importance of endosome-localized actin filaments in endosome motility and positioning (24-27), we wondered whether OTUD1 is involved in actin organization and hereby controls endosome biology. This idea was corroborated by the notion that a small fraction of OTUD1 co-localized with actin and Filamin A at peripheral protrusion structures (Fig. 4c). Furthermore, OTUD1 depleted cells contained a vastly extended actin network, including more and smaller actin fibers, as if the actin organization was perturbed (Fig. 4d). Also, the morphology of these cells was altered, which was especially apparent in glioblastoma U118 cells, where many cells containing spikey but short protrusions (Fig. 4e), suggestive of a defect in cellular organization or altered migratory behavior. To address whether OTUD1-mediated actin reorganization and endosome positioning are coupled, we silenced FLNA, as well as Keap1, another actin-binding protein identified in the mass spec experiment, and analyzed its effect on endosome positioning. Whereas cells appeared more elongated in both cases, no striking effect was observed on endosome positioning (data not shown). Thus, OTUD1 is involved in actin dynamics and endosome positioning, the latter probably independently of FLNA and Keap1.

Discussion

Vesicle transport and delivery of associated cargo is tightly controlled by members

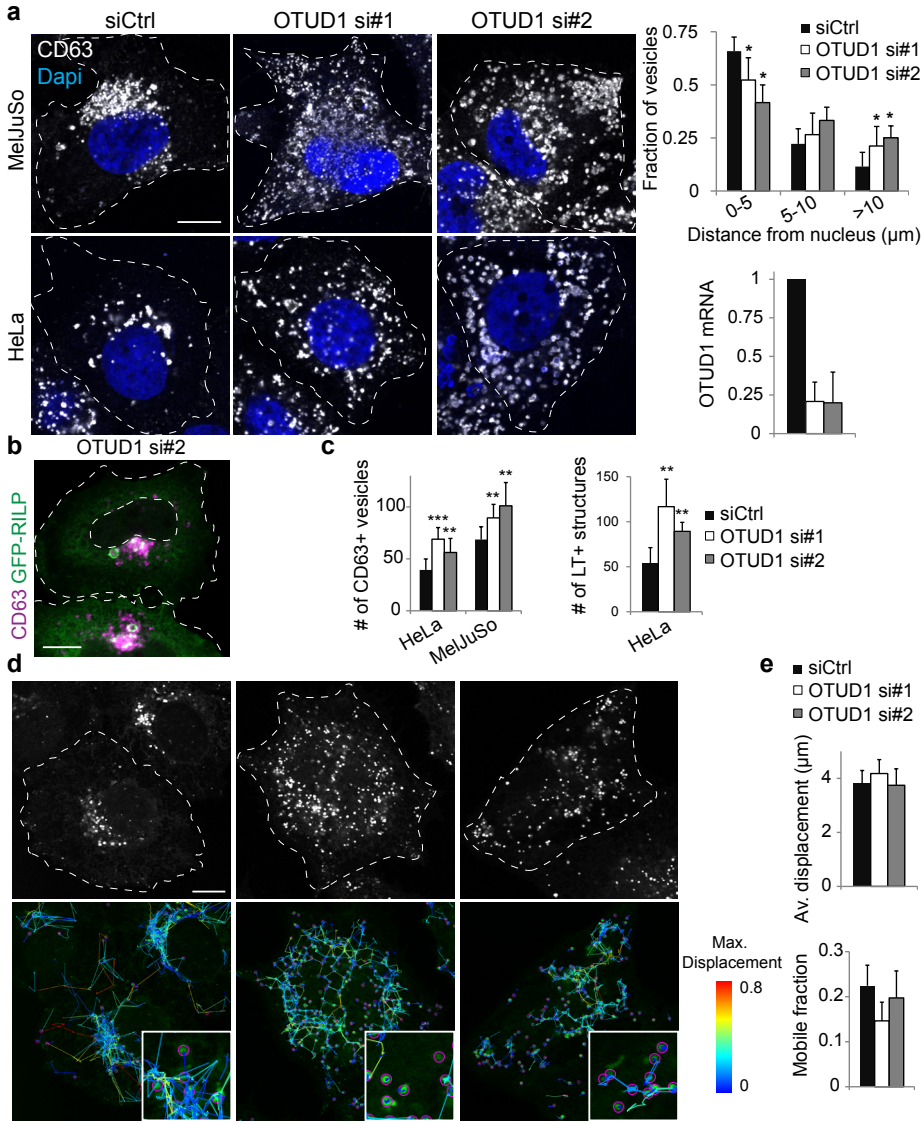

Figure 2: OTUD1 is required for late endosome positioning. *(A) MelJuSo and HeLa cells transfected with indicated siRNAs were fixed and stained for CD63 and DAPI. Bar = 10 µm. Quantification of CD63+ vesicle distance from the nucleus. Fraction of vesicles in each of the categories was quantified in at least 10 cells per experiment, n=3. Bottom right: silencing efficiency of OTUD1 in MelJuSo cells as detected by qRT-PCR. (B) siRNA transfected HeLa cells were transfected with GFP-RILP and fixed and stained for the indicated markers. (C) Amount of CD63+ (antibody staining) or Lysotracker+ (Live cell microscopy) structures in HeLa or MelJuSo cells transfected with the indicated siRNAs. At least 10 cells were counted from at least two independent experiments. (D) Dynamics of lysotracker marked vesicles in HeLa cells transfected with the indicated siRNAs. Confocal image at start of time-lapse is shown on the top, vesicle trajectories over a 240 sec interval are displayed below. Colors of individual vesicle trajectories are compared to the maximal displacement rate (blue=0, red=0.8 of control). Scale bar, 10 µm. (E) Average displacement (µm) for a vesicle during the 240 sec duration of the movie using trackmate. Bottom: quantification of the fraction of mobile vesicles. Vesicles with a total displacement of >5µm during the movie were considered immobile. For both quantifications over 5 fields of cells were imaged over 2 independent experiments.*

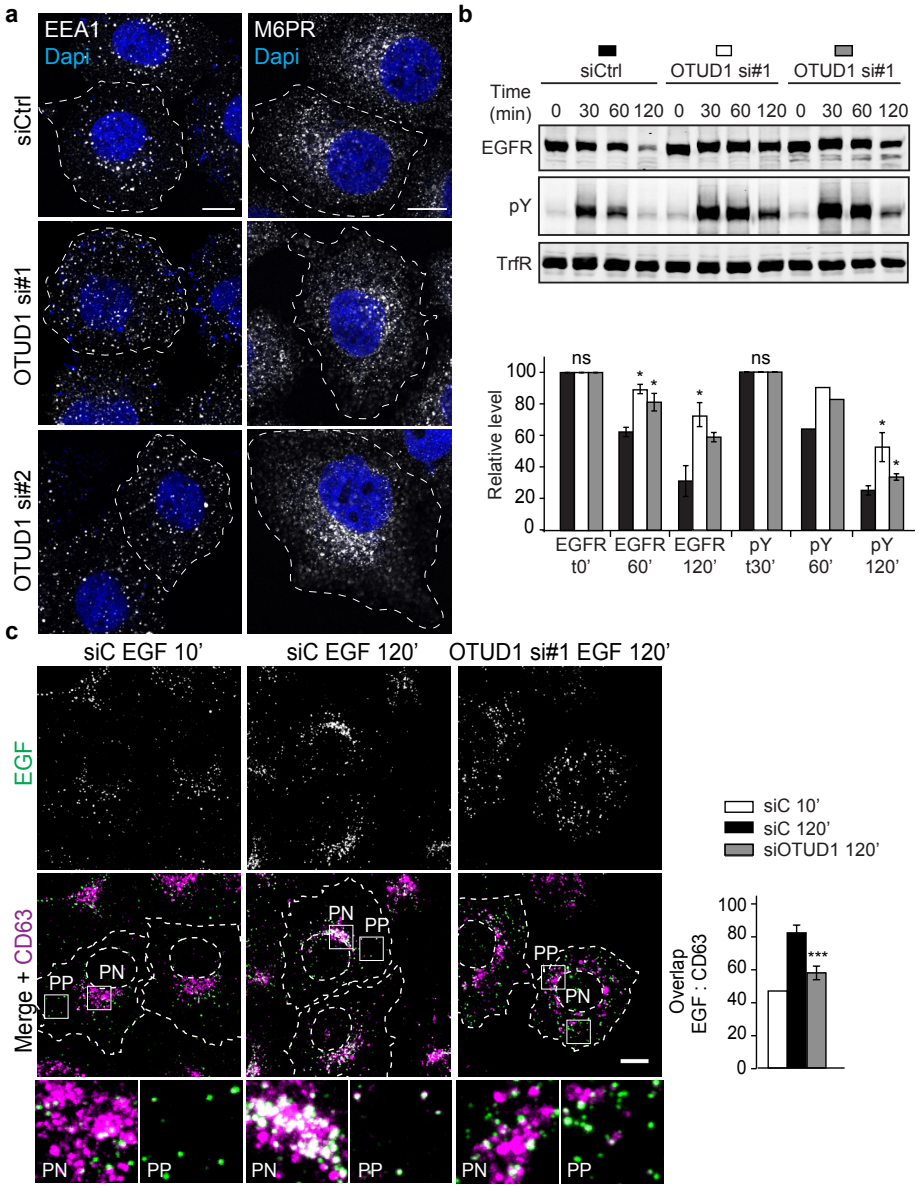

Figure 3: OTUD1 regulates early endosome positioning and EGFR degradation. *(A) HeLa cells were transfected with the indicated siRNAs and fixed and stained for EEA1 or Mannose-6-phosphate receptor (M6PR) and DAPI three days later. Bar = 10 µm. (B) EGFR degradation in control versus OTUD1-depleted HeLa cells. Immunoblots against total (EGFR) and phosphorylated (pY) EGFR, as well as TfR (loading control) along a time course following 20 ng/ml EGF addition (min) are shown. For quantification of EGFR, signal was normalized to corresponding t=0min. (C) Effect of OTUD1 depletion on receptor-mediated trafficking of EGF-555 (green) to the late endosome compartment (CD63, magenta). Representative z projection (3D) overlays at 10 min (left panels) and 120 min (right panels) following stimulation (100 ng/ml) are shown with perinuclear (PN) and peripheral (PP) zooms for control and OTUD1-depleted HeLa cells. Colocalization (Mander's overlap) of EGF with CD63 at 10 min (white) and 120 min (black) following ligand stimulation.*

of the endosomal system, as well as the cytoskeleton and external stimuli. Due to its specific spatiotemporal characteristics, where each vesicle should be controlled on an individual basis, the endocytic system is strongly regulated by dynamic post-translational modifications. Using an RNAi screen we identified novel DUBs that function in the endocytic system. One of these, OTUD1, is required for proper perinuclear localization of both early- and late endosomes and its loss impairs access of endocytosed material to the lysosome. Furthermore, OTUD1 interacts with actin-crosslinking protein FLNA and controls the actin cytoskeletal structure and cell morphology.

Timely delivery of growth receptors, adhesion complexes and autophagic cargo is facilitated by endosomal fusion, fission, sorting and transport events, materializing from different endosomal subsets. Organization of these events occurs at the cellular level by mechanisms regulating endosome positioning, such as the RNF26 system (21), as well as on the individual endosome basis, regulated by for example cargo itself (28). Our data show that loss of OTUD1 leads to a disorganized early- and late endosomal compartment, whereas other endocytic carriers such as the trans-Golgi network remain intact. Furthermore, the timely delivery of activated growth receptors like EGFR to the lysosomal compartment was perturbed, with EGFR accumulating in the early endosomal compartment. Whereas the molecular mechanism by which OTUD1 regulates these events is still unclear, our data suggest regulation at the interplay between the early- and late endosomal compartment, or alternatively of a protein complex that acts on both types of endosomes. Interestingly, the scattered endosome phenotype in combination with impaired degradation is reminiscent of a dysfunctional Rab5-Rab7 conversion, as HOPS perturbations provide a similar phenotype. However, we failed to identify any link between OTUD1 and co-isolated endocytic proteins in our mass spectrometry experiment, arguing for a transient interaction or an indirect effect. Therefore, it will be interesting to identify the substrates of OTUD1, by isolating ubiquitinated proteins accumulating after inactivation of OTUD1. We will then assess which of these proteins may link to the endosomal system, also using the data set that we generated in the earlier genome-wide siRNA screen for factors controlling MHC class II. This functional data set integration will allow unbiased hit selection for further experiments.

Besides controlling the integrity of the endosomal compartment, OTUD1 depleted cells displayed an altered morphology and actin cytoskeleton. OTUD1 knockdown cells contained an extended network of small actin fibers, compared to control cells having more focused, thick actin fibers. This could be the result of a functional interaction with the Filamin proteins, which are known to control actin crosslinking (29, 30). However, recent findings showed that OTUD1 restrains TGFβ-signaling by antagonizing RNF12-mediated ubiquitination of SMAD7, hereby increasing the levels of this inhibitory SMAD protein (Peter ten Dijke, personal communication). This in turn impairs migration and epithelial-to-mesenchymal transition, which is accompanied by extensive actin remodeling, suggesting that the effects of OTUD1 on the actin cytoskeleton are indirect, via alterations in the cellular differentiation state. Interestingly, SMAD7 localizes to endosomes to exert its negative regulation of the TGFβ-pathway (31), suggesting a potential coupling of SMAD signaling to

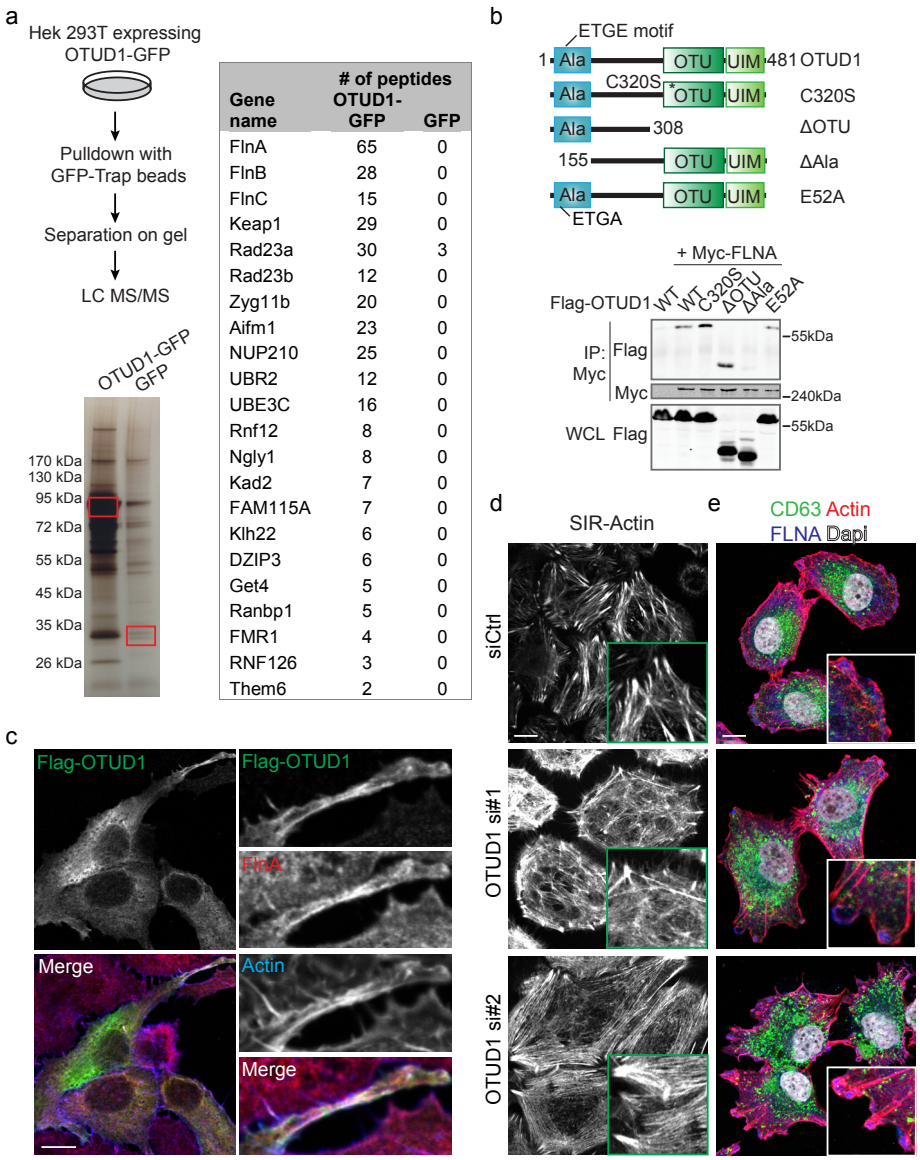

Gene name	# of peptides OTUD1-GFP	GFP
FlnA	65	0
FlnB	28	0
FlnC	15	0
Keap1	29	0
Rad23a	30	3
Rad23b	12	0
Zyg11b	20	0
Aifm1	23	0
NUP210	25	0
UBR2	12	0
UBE3C	16	0
Rnf12	8	0
Ngly1	8	0
Kad2	7	0
FAM115A	7	0
Klh22	6	0
DZIP3	6	0
Get4	5	0
Ranbp1	5	0
FMR1	4	0
RNF126	3	0
Them6	2	0

Figure 4: OTUD1 interacts and colocalizes with Filamin A and alters the actin cytoskeleton. *(A) Hek293T cells expressing GFP or OTUD1-GFP were lysed and immunoprecipitated for GFP using GFP-Trap beads. Associated proteins were visualized by silver stain and bands were subjected to MS/MS analysis. Red box corresponds to molecular weight of the GFP-tagged protein. Proteins identified by at least 2 peptides in the mass spectometer are depicted in the table. (B) Top: domain structure of OTUD1. Bottom: Co-immunoprecipitation for Filamin A (FLNA) with OTUD1. Myc-FLNA was isolated from lysates of HEK293T cells co-overexpressing indicated Flag-OTUD1 constructs using Myc-Trap beads. Western blot filters were probed for isolated Myc-tagged proteins, and the associated Flag-OTUD1. (C) HeLa cells transfected with Flag-OTUD1 were fixed and stained for the indicated markers. Bar = 10 µm. (D) HeLa cells transfected with the indicated siRNAs were imaged under the microscope using the SIR-actin probe. Still image is represented, bar = 10 µm. (E) U118 cells transfected with the indicated siRNAs were fixed and stained for the indicated markers. Bar = 10 µm.*

the effect of OTUD1 on the endosomal pathway. Alternatively, Filamin A has been shown to stimulate TGFβ-signaling by allowing phosphorylation of SMAD2 (32), which is antagonized by SMAD7 (33). Filamin A could thus interact with OTUD1 to prevent de-ubiquitination of SMAD7. Similarly, depletion of Keap1, another actin- and OTUD1-interacting protein, increases SMAD7 protein levels and attenuates TGFβ-signaling (34), raising the possibility that Keap1 inhibits OTUD1. It will be interesting to investigate the potential interplay between actin organizers and OTUD1 in relation to TGFβ-signaling, as well as the function of OTUD1 recruitment to different sites of action.

In summary, our experiments identify the DUB OTUD1 as critical in the organization and function of the endocytic compartment. Furthermore, MHC class II expression is controlled by OTUD1, as well as organization of the actin cytoskeleton. Additional experiments are required to dissect the underlying molecular mechanisms of action.

Materials and methods

Cell culture and constructs

MelJuSo cells and MelJuSo cells stably expressing GFP-Ubiquitin or GFP-HLA-DRα (35) were cultured in IMDM supplemented with 10% FCS, HeLa and Hek293T cells in DMEM with 10% FCS. The following constructs were obtained from addgene: Myc-FLNA (#8982), Flag-OTUD1 (#22553). GFP-RILP was described previously (36). OTUD1 and indicated mutants were cloned into a Flag-C1 vector.

Reagents and antibodies

For lysosomal staining Lysotracker green (Molecular probes) was used, for actin staining SIR-Actin (TeBu Bio). Antibodies used: rabbit anti-MHCII (1:100), rabbit anti-GFP (1:1000), mouse anti-CD63 (1:500) and rabbit anti-CD63 (1:100) (all described in (36)), mouse anti-HA (Covance 16B12, 1:1000), rat anti-HA 3F10 (Roche, 1:200), mouse anti-M6PR, rabbit anti-FLNA (all from Abcam, both 1:100), mouse anti-EEA1 , mouse anti-Transferrin receptor (Invitrogen, 1:100 confocal, 1:1000 western blot), rabbit anti-Flag F7425 and mouse anti-Flag M2 (Sigma, 1:1000), rabbit anti-EGFR (Millipore, 1:1000), mouse anti-phosphotyrosine (pY; 4G10 Millipore, 1:1000), actin was stained with Phalloidin-Alexa 647 (Life Technologies). Secondary antibodies (goat anti-mouse Alexa 405/488/568/647, goat anti-rabbit Alexa 488/568/647, donkey anti-goat Alexa 488/568, donkey anti-mouse Alexa 488/555/647 and donkey anti-rabbit Alexa 488/647) were purchased from Life Technologies and donkey anti-rat CF568 from Biotium (all 1:200).

Transfections

For expression studies, MelJuSo and HeLa cells were transfected using Effectene (Qiagen) according to the manufacturer's instructions. Cells were transfected one day before fixation or lysis. Hek293T cells were transfected using polyethylenimine (PEI). For siRNA mediated depletion, cells were reverse transfected with DharmaFECT transfection reagent #1 and 50 nM siRNA of the Human siGenome SMARTpool, Dharmacon, according to the manufacturer's protocol. siRNA sequences for OTUD1: #1 5'-ACGAAGAACTTGCCAAATC-3' and #2 5'-TATCATCGCTGCTGCCCCAA -3'. Briefly, siRNAs and DharmaFECT were mixed and

incubated for 20 minutes in a culture well, after which cells were added and left to adhere (reverse transfection). Three days later, cells were fixed and stained or lysed for biochemical analysis.

Flow Cytometry

Three days after siRNA transfections as described above, cells were trypsinized and stained with Cy3-labeled L243 antibody, described in (16), and analyzed using flow cytometry (BD FACSArray). For staining of total pMHCII levels, cells were fixed with 2% formaldehyde and permeabilized using 0.125% Saponin before staining, which was also used during antibody washes. Data were normalized to the control (siCtrl transfected cells) and z-scores were calculated using the standard deviations of the controls. All hits with z-scores > 2.5 were included in follow up analysis.

EGFR degradation assays

Ligand-mediated turnover of EGFR was assayed as previously described using 20ng/ml EGF (21). Receptor abundance at each indicated time-point following stimulation was quantified relative to Transferrin receptor and expressed as a fraction of EGFR at t=0 for each condition. Receptor phosphorylation was expressed relative to the maximal activation achieved in control cells (siC).

Co-immunoprecipitation and Western blotting

For co-immunoprecipitation experiments, Hek293T cells were lysed in lysis buffer (0.5% NP-40, 5% glycerol, 150mM NaCl, 50mM Tris-HCl pH8.0, 5mM MgCl2 supplemented with complete EDTA-free Protease Inhibitor Cocktail (Roche)) and cleared by centrifugation. Lysates were incubated with GFP-Trap beads (Chromotek) or protein G-Sepharose 4 FF resin with the indicated antibodies and after incubation washed extensively with lysis buffer before addition of sample buffer (2% SDS, 10% glycerol, 5% β-mercaptoethanol, 60mM Tris-HCl pH 6.8 and 0.01% bromophenol blue).

For whole cell lysate analyses, cells were lysed directly in sample buffer. Proteins were separated by SDS-PAGE and transferred to Western Blot filters. Blocking of the filter and antibody incubations were done in PBS supplemented with 0.1 (v/v)% Tween and 5% (w/v) milk powder. Blots were imaged using the Odyssey Imaging System (LI-COR) or ChemiDoc (Bio-Rad).

Mass spectrometry

Samples from immune-precipitated GFP-tagged proteins were separated by SDS-PAGE and were silver stained (Invitrogen). Selected bands (and the same region in the GFP control lane as negative controls) were cut from the silver stained gel and subjected to reduction with dithiothreitol, alkylation with iodoacetamide and in-gel trypsin digestion using a Proteineer DP digestion robot (Bruker). Tryptic peptides were extracted from the gel, lyophilized, dissolved in 95/3/0.1 v/v/v water/acetonitril/formic acid and subsequently analyzed by online nanoHPLC MS/MS using an 1100 HPLC system (Agilent Technologies), as previously described (Meiring et al., 2002). Peptides were trapped at 10 µl/min on a 15mm column (100µm ID; ReproSil-Pur C18-AQ, 3 µm, Dr. Maisch GmbH) and eluted to a 200 mm column (50µm ID; ReproSil-Pur C18-AQ, 3 µm) at 150 nl/min. All columns were packed in house. The column was developed with a 30min gradient from 0 to 50% acetonitrile in 0.1% formic acid. The end of the nanoLC column was drawn to a tip (5-µm ID),

from which the eluent was sprayed into a 7tesla LTQ-FT Ultra mass spectrometer (Thermo Electron). The mass spectrometer was operated in data-dependent mode, automatically switching between MS and MS/MS acquisition. Full scan MS spectra were acquired in the FT-ICR with a resolution of 25,000 at a target value of 3,000,000. The two most intense ions were then isolated for accurate mass measurements by a selected ion-monitoring scan in FT-ICR with a resolution of 50,000 at a target accumulation value of 50,000. Selected ions were fragmented in the linear ion trap using collision-induced dissociation at a target value of 10,000. In a post-analysis process, raw data were first converted to peak lists using Bioworks Browser software v3.2 (Thermo Electron), and then submitted to the Swissprot database version 51.6 (257,964 entries), using Mascot v. 2.2.04 (www.matrixscience.com) for protein identification. Mascot searches were with 2 ppm and 0.8 Da deviation for precursor and fragment mass, respectively, and trypsin as enzyme. Protein was finally sorted and compared using Scaffold software version 3.0.1 (www. proteomesoftware.com).

cDNA synthesis and qPCR

RNA isolation, cDNA synthesis and quantitative RT-PCR were performed according to the manufacturer's (Roche) instructions. Signal was normalized to GAPDH and calculated using the Pfaffl formula. Primers used for detection were: GAPDH fw: 5'-TGTTGCCATCAATGACCCCTT-3', GAPDH rv: 5'-CTCCACGACGTACTCAGCG-3', HLA-DRα fw: 5'- -3', HLA-DRα rv: 5'- -3', IRF1 fw: 5'-GCACCAGTGATCTGTACAAC-3', IRF1 rv: 5'-GCTCCTCCTTACAGCTAAAG-3', CIITA fw: 5'-CCTGCTGTTCGGGACCTAAA-3, CIITA rv: 5'-GGATCCGCACCAGTTTGG-3', OTUD1 fw: 5'-CCTAGTATTTGGCTCAGTTGG-3', OTUD1 rv: 5'-TTGTCGTACTCTGGGTTAGG-3'.

Confocal microscopy

Cells were seeded on coverslips, transfected 18 hours later and treated as indicated. 24 hrs later, cells were fixed in 3.7% formaldehyde for 10 min and permeabilized in ice-cold methanol (for LC3 stainings) for 2 minutes or in 0.1% Triton-X100 for 10 minutes. Alternatively, cells were fixed and permeabilized in ice-cold methanol for 2 minutes for Tubulin stainings. Staining was performed with the antibodies mentioned above and DAPI (Invitrogen) to stain DNA. Images were acquired using a Leica TCS SP5 confocal microscope (Leica Microsystems, Wetzlar, Germany) at 63x magnification. For live-cell imaging, the microscope was equipped with a climate control chamber and cells were imaged for 3 minutes with ~6 frames per minute. Images were quantified using Image J plugin Jacob for Mander's coefficient calculations or FIJI's Trackmate plugin for live-cell imaging and processed using Adobe Photoshop and Illustrator.

Acknowledgements

We thank the NKI and LUMC microscopy facility, the NKI FACS facility and the NKI Robotics and Screening facility, with special thanks to Ben Morris for all his help with hit validations. Also, members of the Neefjes group for critical discussions, Nico Ong for developing electron micrographs, Lennert Janssen for help with cloning. This work was supported by the Institute of Chemical Immunology (ICI), an NWO Gravitation project funded by the Ministry of Education, Culture and Science

of the government of the Netherlands and a European Research Council (ERC) advanced grant awarded to J.N.

References

1. J. Neefjes, M. L. Jongsma, P. Paul, O. Bakke, Towards a systems understanding of MHC class I and MHC class II antigen presentation. Nat Rev Immunol 11, 823-836 (2011).
2. R. H. Wijdeven, J. M. Bakker, P. Paul, J. Neefjes, Exploring genome-wide datasets of MHC class II antigen presentation. Molecular immunology 55, 172-174 (2013).
3. M. M. Fernando et al., Defining the role of the MHC in autoimmunity: a review and pooled analysis. PLoS Genet 4, e1000024 (2008).
4. E. R. Unanue, V. Turk, J. Neefjes, Variations in MHC Class II Antigen Processing and Presentation in Health and Disease. Annual review of immunology 34, 265-297 (2016).
5. W. Reith, S. LeibundGut-Landmann, J. M. Waldburger, Regulation of MHC class II gene expression by the class II transactivator. Nat Rev Immunol 5, 793-806 (2005).
6. J. Schneppenheim et al., The intramembrane protease SPPL2a promotes B cell development and controls endosomal traffic by cleavage of the invariant chain. J Exp Med 210, 41-58 (2013).
7. D. R. Beisner et al., The intramembrane protease Sppl2a is required for B cell and DC development and survival via cleavage of the invariant chain. J Exp Med 210, 23-30 (2013).
8. W. Pos et al., Crystal structure of the HLA-DM-HLA-DR1 complex defines mechanisms for rapid peptide selection. Cell 151, 1557-1568 (2012).
9. C. Paludan et al., Endogenous MHC class II processing of a viral nuclear antigen after autophagy. Science (New York, N.Y.) 307, 593-596 (2005).
10. D. Schmid, M. Pypaert, C. Munz, Antigen-loading compartments for major histocompatibility complex class II molecules continuously receive input from autophagosomes. Immunity 26, 79-92 (2007).
11. D. Komander, M. J. Clague, S. Urbe, Breaking the chains: structure and function of the deubiquitinases. Nature reviews. Molecular cell biology 10, 550-563 (2009).
12. O. Kerscher, R. Felberbaum, M. Hochstrasser, Modification of proteins by ubiquitin and ubiquitin-like proteins. Annual review of cell and developmental biology 22, 159-180 (2006).
13. R. C. Piper, I. Dikic, G. L. Lukacs, Ubiquitin-dependent sorting in endocytosis. Cold Spring Harbor perspectives in biology 6, (2014).
14. M. J. Clague, S. Urbe, Integration of cellular ubiquitin and membrane traffic systems: focus on deubiquitylases. The FEBS journal, (2017).
15. M. H. Wright, I. Berlin, P. D. Nash, Regulation of endocytic sorting by ESCRT-DUB-mediated deubiquitination. Cell Biochem Biophys 60, 39-46 (2011).
16. P. Paul et al., A Genome-wide multidimensional RNAi screen reveals pathways controlling MHC class II antigen presentation. Cell 145, 268-283 (2011).
17. I. Berlin, H. Schwartz, P. D. Nash, Regulation of epidermal growth factor receptor ubiquitination and trafficking by the USP8.STAM complex. The Journal of biological chemistry 285, 34909-34921 (2010).
18. I. Berlin, K. M. Higginbotham, R. S. Dise, M. I. Sierra, P. D. Nash, The deubiquitinating enzyme USP8 promotes trafficking and degradation of the chemokine receptor 4 at the sorting endosome. The Journal of biological chemistry 285, 37895-37908 (2010).
19. T. E. Mevissen et al., OTU deubiquitinases reveal mechanisms of linkage specificity and enable ubiquitin chain restriction analysis. Cell 154, 169-184 (2013).
20. A. P. Carneiro et al., A putative OTU domain-containing protein 1 deubiquitinating enzyme is differentially expressed in thyroid cancer and identifies less-aggressive tumours. British journal of cancer 111, 551-558 (2014).
21. M. L. Jongsma et al., An ER-Associated Pathway Defines Endosomal Architecture for Controlled Cargo Transport. Cell 166, 152-166 (2016).
22. M. E. Sowa, E. J. Bennett, S. P. Gygi, J. W. Harper, Defining the human deubiquitinating enzyme interaction landscape. Cell 138, 389-403 (2009).
23. G. Liu et al., Cytoskeletal protein ABP-280 directs the intracellular trafficking of furin and modulates proprotein processing in the endocytic pathway. The Journal of cell biology 139, 1719-1733 (1997).
24. M. Fernandez-Borja, L. Janssen, D. Verwoerd, P. Hordijk, J. Neefjes, RhoB regulates endo-

some transport by promoting actin assembly on endosomal membranes through Dia1. Journal of cell science 118, 2661-2670 (2005).
25. A. L. Zajac, Y. E. Goldman, E. L. Holzbaur, E. M. Ostap, Local cytoskeletal and organelle interactions impact molecular-motor- driven early endosomal trafficking. Current biology : CB 23, 1173-1180 (2013).
26. M. Anitei, B. Hoflack, Bridging membrane and cytoskeleton dynamics in the secretory and endocytic pathways. Nature cell biology 14, 11-19 (2011).
27. J. Taunton et al., Actin-dependent propulsion of endosomes and lysosomes by recruitment of N-WASP. The Journal of cell biology 148, 519-530 (2000).
28. J. Huotari, A. Helenius, Endosome maturation. The EMBO journal 30, 3481-3500 (2011).
29. G. M. Popowicz, M. Schleicher, A. A. Noegel, T. A. Holak, Filamins: promiscuous organizers of the cytoskeleton. Trends in biochemical sciences 31, 411-419 (2006).
30. F. Nakamura, T. P. Stossel, J. H. Hartwig, The filamins: organizers of cell structure and function. Cell adhesion & migration 5, 160-169 (2011).
31. G. M. Di Guglielmo, C. Le Roy, A. F. Goodfellow, J. L. Wrana, Distinct endocytic pathways regulate TGF-beta receptor signalling and turnover. Nature cell biology 5, 410-421 (2003).
32. A. Sasaki, Y. Masuda, Y. Ohta, K. Ikeda, K. Watanabe, Filamin associates with Smads and regulates transforming growth factor-beta signaling. The Journal of biological chemistry 276, 17871-17877 (2001).
33. H. Hayashi et al., The MAD-related protein Smad7 associates with the TGFbeta receptor and functions as an antagonist of TGFbeta signaling. Cell 89, 1165-1173 (1997).
34. I. G. Ryoo, H. Ha, M. K. Kwak, Inhibitory role of the KEAP1-NRF2 pathway in TGFbeta1-stimulated renal epithelial transition to fibroblastic cells: a modulatory effect on SMAD signaling. PloS one 9, e93265 (2014).
35. N. P. Dantuma, T. A. Groothuis, F. A. Salomons, J. Neefjes, A dynamic ubiquitin equilibrium couples proteasomal activity to chromatin remodeling. The Journal of cell biology 173, 19-26 (2006).
36. R. van der Kant et al., Late endosomal transport and tethering are coupled processes controlled by RILP and the cholesterol sensor ORP1L. Journal of cell science 126, 3462-3474 (2013).